Journal of Materials Chemistry A

Accepted Manuscript

ROYAL SOCIETY OF CHEMISTRY

www.rsc.org/materialsA

Journal Name

ARTICLE

Perovskite oxides for application in thermochemical air separation and oxygen storage

Received 00th January 20xx,
Accepted 00th January 20xx

DOI: 10.1039/x0xx00000x

www.rsc.org/

J. Vieten[a], B. Bulfin[a], F. Call[a], M. Lange[a], M. Schmücker[b], A. Francke[b], M. Roeb[a], C. Sattler[a]

Perovskites $AMO_{3-\delta}$ are ideal for thermochemical air separation due to their oxygen nonstoichiometry δ, which can be varied by changing the temperature and oxygen partial pressure. We show in this work how materials can be selected for chemical looping air separation from thermodynamic considerations and present thermogravimetric experiments carried out on (Ca,Sr) ferrites and manganites, and doped variants, all synthesized via a citric acid auto-combustion method. $SrFe_{0.95}Cu_{0.05}O_{3-\delta}$ and $Ca_{0.8}Sr_{0.2}MnO_{3-\delta}$ show the best gravimetric oxygen storage capacity of all tested materials at T < 1200 °C. The redox reactions are completed in < 1 min in air and highly reversible. A significant re-oxidation reaction of reduced samples was observed at temperatures as low as 250 °C at an oxygen partial pressure of 0.16 bar. We studied phase formation via XRD and the lattice expansion during reduction via *in-situ* XRD experiments. The objective is to validate the potential and boundary conditions of such materials to pave the way for competitive air separation based on thermochemical cycling.

Perovskite materials have attracted great attention in the past years in many different fields of materials science due to their interesting physical properties and wide range of applications. Oxide perovskite compounds with the general formula AMO_3 can be applied for instance as solid oxide fuel cell (SOFCs) cathodes, [1, 2] for thermochemical CO_2 and H_2O splitting, [3-5] for oxygen selective membranes, [6-8] and as catalysts for fuel production, for oxidation of organic compounds, [9, 10] and for automotive applications (exhaust gas treatment). [11, 12]

The two cation sites of perovskites, referred to in the following as A and M, are occupied by a larger A^{m+} and a smaller M^{n+} ion. [13] A is typically an alkaline earth, alkali, or rare earth metal, whereas the M species are in most cases transition metal cations. The redox properties of these perovskite oxides are particularly interesting if multivalent atomic species are involved. Given an alkaline earth metal cation A^{2+} and a transition metal M^{4+}, in many cases the M ions can be reduced to M^{3+}. In case of complete M^{4+} to M^{3+} reduction, the perovskite AMO_3 is converted to its defect-ordered variant (brownmillerite, $A_2M_2O_5$) while oxygen is released. [14, 15] The perovskite crystal structure, however, also allows a considerable M^{4+} to M^{3+} reduction resulting in an oxygen nonstoichiometry δ, where δ = 0-0.5 for $A^{2+}M^{3/4+}O_{3-\delta}$:

$$AMO_3 \overset{p_{O_2},T}{\longleftrightarrow} AMO_{3-\delta} + \frac{\delta}{2} O_2 \qquad (1)$$

Depending on partial pressure p_{O_2} and temperature *T,* perovskite defect structures with certain δ, brownmillerite phases or phase mixtures will be formed. During reduction and oxidation, only small structural changes occur in most cases, thus fast redox kinetics and a high reversibility are achieved. [16] The high oxygen ion conductivity of perovskites contributes to their fast redox kinetics. [17, 18] Moreover, the perovskite structure is highly versatile and shows an enormous variety of compositions. [13] This allows the exchange of metal cations in order to tune the perovskite properties over a wide range, typically without significant changes in the basic crystal structural motif.

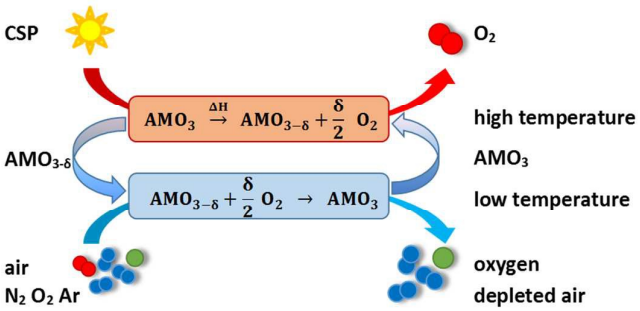

Fig. 1 Thermochemical air separation process using nonstoichiometric perovskites AMO_3. At high temperatures, provided for instance by concentrated solar power (CSP), the perovskites are partially reduced, leading to an increase in oxygen vacancy concentration δ under the release of pure oxygen. The reduced perovskites can then be used to remove oxygen from an air stream at lower temperatures while they are re-oxidized.

[a] Institute of Solar Research, and [b]Institute of Materials Research, Deutsches Zentrum für Luft- und Raumfahrt/German Aerospace Center—DLR, Linder Höhe, 51147 Köln, Germany

Electronic Supplementary Information (ESI) available: Detailed information on the synthesis route, X-Ray diffractograms, detailed data of *in-situ* XRD, further thermogravimetric data, long term studies, summary tables of all materials and video of auto-combustion reaction.

The redox properties of perovskites are particularly useful for the thermochemical capture and release of oxygen from a gas mixture such as air, [19-24] as shown in **Fig.1**. This thermochemical cycling is referred to as chemical looping, [21, 25] and can also be applied similarly for H_2O or CO_2 splitting. [3-5, 26, 27] At high temperatures and/or low oxygen partial pressures, the perovskite is reduced and the oxygen nonstoichiometry δ is increased while pure oxygen is released. The reduced perovskites can then be re-oxidized at lower temperatures and/or higher oxygen partial pressures, which leads to a regeneration of the starting material. In this step, oxygen can be captured from a gas mixture, yielding a stream of oxygen-deficient gas. If CO_2, H_2O and trace gases are removed by other means, a stream of inert gas can be produced from air, which is highly valuable for many industrial applications. This process could be an environmentally friendly alternative to the Thomson-Linde process, [28] where air is separated by cryogenic distillation. A substantial reduction of industrial greenhouse gas emissions can thus reached if renewable heat sources like concentrated solar power (CSP) are used in countries with high solar radiation. [21, 29, 30] Using this process as a nitrogen source can be particularly relevant for the production of ammonia, [29] which is attributed to at least 1 % of the worldwide primary energy consumption. [31]

Previous studies on perovskites and brownmillerites as oxygen storage or air separation materials show the potential of these materials to reversibly store substantial amounts of oxygen. [19, 20, 32, 33] Ezbiri et al. show how perovskites exhibiting an oxygen affinity that is high enough to absorb oxygen from air but low enough to be easily reduced can be found via DFT (density functional theory) calculations. [19] However, the synthesis and the complete re-oxidation of the presented $SrCoO_{3-\delta}$ require high oxygen pressures, and the gravimetric oxygen storage capacity in air is therefore limited.

Materials selection principles

We focus on perovskites and brownmillerites with the general composition $A^{2+}M^{3/4+}O_{3-\delta}$ in the following, as many transition metals show stable oxidation states of both +3 and +4, allowing a large variety of compositions. For oxygen enrichment, production, and storage, as well as for air separation applications, those perovskites should show a high ratio of oxygen storage capacity to heat capacity in order to reduce the thermal energy transferred in each cycle. As the heat capacity of new compounds is often not known, in our screening we simplify this requirement to a high gravimetric oxygen storage capacity. We therefore chose Ca^{2+} and Sr^{2+} as cations on the A^{2+} site, and the lightest transition metals (3d transition metals) for the $M^{3+/4+}$ site. The oxygen affinity of the redox material should be low enough to allow thermal reduction in air at moderate temperatures (below 1200 °C in this work), but high enough to enable a full re-oxidation of the reduced form to its initial state in air. [19] A measure for the reducibility of an oxide is its reduction enthalpy ΔH_{red}. A low reduction enthalpy will result in a lower onset temperature for the reduction reaction (see Eq. 3). The enthalpies for the complete reduction from the perovskite to the brownmillerite phase

$$4\,\mathrm{AMO_3} \rightarrow 2\,\mathrm{A_2M_2O_5} + \mathrm{O_2} \qquad (2)$$

per mol of O_2 were compiled with the help of *The Materials Project*, [34] a web interface providing thermodynamic data based on DFT calculations. [34-36]

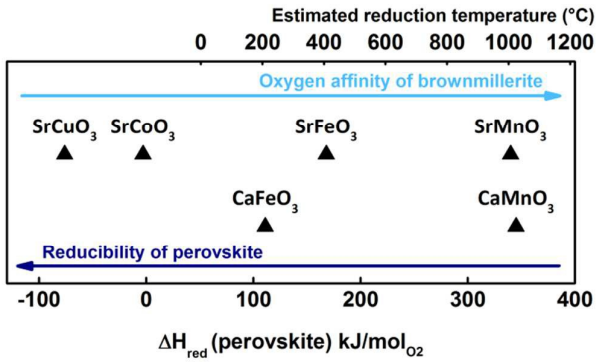

Fig. 2 Theoretical reduction enthalpies ΔH_{red} per mol of O_2 of different $A^{2+}M^{3/4+}O_3$ perovskites for a complete reduction to the brownmillerite phase $A^{2+}M^{3/4+}O_{2.5}$ along with the estimated reduction temperatures in air. Reaction enthalpies based on calculations in The Materials Project. [34-36] The estimated reduction temperature in air is determined neglecting configurational entropy contributions to ΔS (see text).

Fe, Co, Cu, and Mn perovskites and brownmillerites have known structures and reduction enthalpies, and are therefore considered in the following. Mn and Fe show considerably stable oxidation states of both +3 and +4. Co and Cu form Sr-based perovskites that are only stable at high oxygen partial pressures, which is indicated by their negative ΔH_{red} (see **Fig. 2**). This behavior is attributed to the relative instability of Co(IV) [37] and Cu(IV) [38]. $SrCoO_{2.5}$ has been investigated for oxygen separation applications, but its oxygen storage capacity is limited as it cannot be re-oxidized completely to $SrCoO_3$ in air, as mentioned before. [19] $SrCuO_3$ would show Cu in an unusual +4 state, [38] of which the existence in a perovskite structure has been proposed for $\mathrm{La_{1-x}Sr_xCuO_3}$. [39] However, a perovskite with all Cu ions in the oxidation state +4 like $SrCuO_3$ has not been produced as a bulk material yet and is expected to be unstable in a thermodynamic sense. [34, 40] Nevertheless, partial substitution of the M^{4+} cations with Cu or Co could increase the reducibility of ferrites and manganites.

In order for the reduction reaction to proceed spontaneously, its Gibbs free energy $\Delta G°$ needs to be less than zero, according to

$$\Delta H° - T \cdot \Delta S° = \Delta G°(T) < 0 \qquad (3)$$

Assuming in first approximation that the entropy change ΔS^0 is only attributed to the release of oxygen gas, and thus using the partial molar entropy of oxygen ${}^{\circ}S_{O_2}$ as calculated with the help of the Shomate equation, [41, 42] it is possible to get a rough estimate of

the expected reduction temperature. However, the configurational entropy changes due to oxygen vacancy formation in the lattice may lead to large deviations of the actual reduction temperature from this first estimate. Moreover, the position of the chemical equilibrium (Eq. 2) is dependent on the oxygen partial pressure p_{O_2}. The relation between ΔG at equilibrium at a given p_{O_2} to $\Delta G°(T)$ at the reference pressure $p° = 1$ bar is given by:

$$\Delta G(p_{O_2}, T) = \Delta G°(T) - RT \cdot \ln\left(\frac{p_{O_2}}{p°}\right) \quad (4)$$

Eq. 4 can be rearranged with the help of Eq. 3 to yield an expression for the equilibrium ($\Delta G = 0$) oxygen partial pressure in terms of the enthalpy and entropy values.

$$\frac{p_{O_2}}{p°} = \exp\left(\frac{\Delta S°}{R}\right)\exp\left(\frac{-\Delta H°}{RT}\right) \quad (5)$$

Comparing different materials with different reduction enthalpy $\Delta H°$ at a given temperature T, and under the assumption of comparable $\Delta S°$ values, it can be stated that a higher $\Delta H°$ leads to a lower equilibrium partial pressure of oxygen (p_{O_2}) for a given temperature. Therefore, a material with high $\Delta H°$ can be used to achieve a high purity of the output gases in an air separation device, but the required energy input per mol of removed oxygen is higher. An air separation process would therefore ideally consist of at least two steps with two different air separation materials. In the first step, an easily reducible material is used to remove the bulk of the oxygen with a relatively low energy consumption. A material with larger $\Delta H°$, can then be used to achieve very low partial pressures, with only a small additional energy cost, due to the small amount of oxygen that needs to be removed.

The reduction enthalpies of different perovskites per mol of O_2, as well as the estimated reduction temperatures in air are shown in **Fig. 2**. Manganites are expected to require high temperatures for reduction (~ 1000 °C) and should also allow very low partial pressures to be achieved during oxidation. Ferrites on the other hand can be reduced at lower temperatures and thus could be used for removing the bulk of the oxygen from an air stream. This is consistent with experimental data in the literature. [43-45] $SrCuO_x$ and $SrCoO_x$ are most stable in the brownmillerite state (x = 2.5), and even $CaFeO_{2.5}$ can only be oxidized substantially under elevated oxygen pressures. [46, 47] The oxygen affinity of these reduced species is low and the absorption of oxygen from a stream of air is therefore expected to be inefficient.

As a conclusion from the materials selection process and based on the estimated reduction temperatures, Fe and Mn containing perovskites are regarded as best suitable for low and high temperature air separation, respectively. Therefore, the corresponding materials were synthesized and investigated with respect to air separation and oxygen storage applications. Their properties were optimized by compositional modifications and solid solution formation.

Results and Discussion

$SrFeO_{3-\delta}$ and Cu-containing derivatives

The synthesis of $SrFeO_{3-\delta}$ yielded a grey and sintered substance with metallic appearance, which could easily be powdered in a mortar. According to phase analysis by XRD (see supplementary information), a mixture of $SrFeO_{2.875}$ and $SrFeO_{2.75}$ was formed as expected. [43, 44] Both phases show very similar diffraction patterns. The X-Ray diffraction pattern could be refined in space group No. 65 from the *International Tables* (*Cmmm,* orthorhombic, $SrFeO_{2.75}$ [48]), and the refined crystal parameters showed small deviations from the theoretical values, which may be attributed to the different oxygen stoichiometry.

Based on the previous theoretical considerations and on studies of other authors on Cu containing perovskites, [39, 40] it seems likely that the partial substitution of Fe by Cu in a perovskite could increase its reducibility. For this reason, replacement of 5, 8, 10, 15, and 20 at% Fe by Cu was attempted. The position of the reflections in the XRD did not change upon addition of Cu. The ionic radius of Cu^{4+} ions (if present) is yet unknown, but the ionic radii of Cu^{3+} and Fe^{3+} in 6-fold coordination are almost identical (68 pm and 69 pm, respectively [49]). Therefore, both species are expected to form solid solutions readily, and a difference in lattice parameters by addition of Cu was not detected.

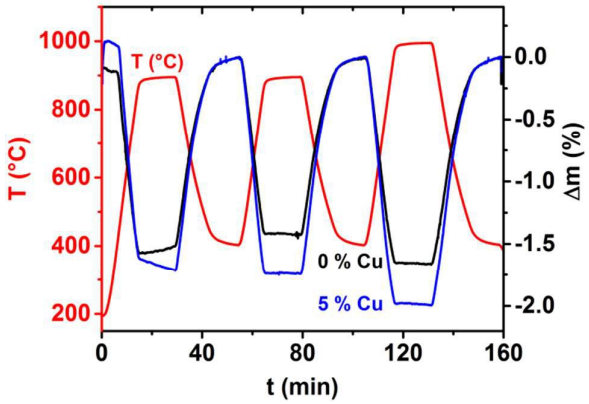

Fig. 3 Thermogravimetric analysis of $SrFeO_{3-\delta}$ (black) and $SrFe_{0.95}Cu_{0.05}O_{3-\delta}$ (blue) at p_{O2} = 0.16 bar and with reduction temperatures of 900 and 1000 °C (last cycle). The exchange of 5 % Fe by Cu leads to a significant increase of the reducibility.

Thermogravimetric experiments show an increased reducibility of the Cu-containing samples with respect to pure $SrFeO_{3-\delta}$. Especially the samples with 5 – 10 % Cu show significant increases in the gravimetric mass changes upon reduction. The replacement of 5 % Fe by Cu led to the most significant increase in oxygen storage capacity. The gravimetric mass change between the oxidized and reduced form increases from 1.68 (no Cu) to 1.98 % (5 % Cu, see **Fig. 3**), whereas samples with 8, 10, 15, or 20 % Cu on the $M^{3/4+}$ site showed slightly lower redox mass changes of 1.88, 1.93, 1.82, and 1.72 %, respectively. Samples with 20 % Cu show the additional minor impurities according to powder XRD (see Supporting

Information Fig. S3). The higher reducibility of Cu containing samples can be attributed to a lower reduction enthalpy, higher entropy changes during reduction, or a combination of both. Further studies are required to elucidate the thermodynamic background of this outcome. The reduction onset at ~ 400 °C is in good agreement with our theoretical estimate and indeed with literature data for pure $SrFeO_{3-\delta}$. [16, 44]

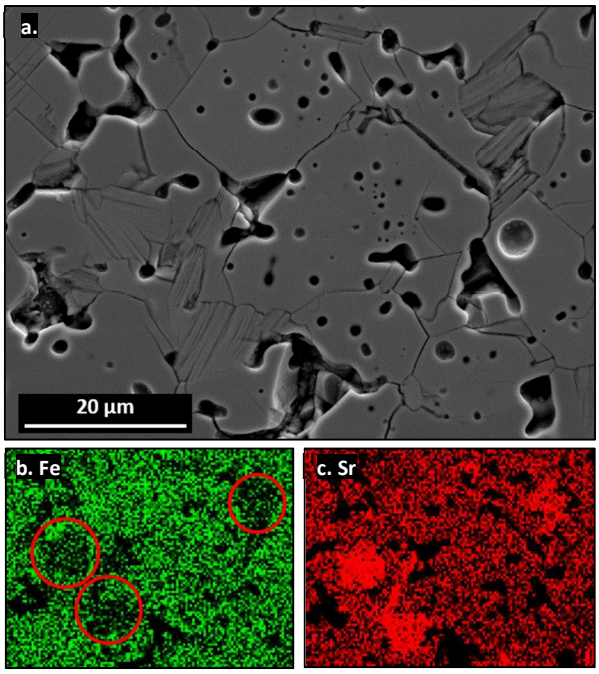

Fig. 4 Phase analysis of annealed and cleaved $SrFe_{0.95}Cu_{0.055}O_{3-\delta}$ pellets. a. SEM image, b. Elemental distribution of Fe ($K_{\alpha1}$ signal), c. Elemental distribution of Sr ($L_{\alpha1}$ signal). Fe poor (red circles) and Sr rich regions indicate the presence of a side phase.

SEM and EDS analysis of annealed and polished pellets prepared from the '5 % Cu' sample revealed the presence of at least one side phase which is Sr rich and Fe poor (see **Fig. 4**), next to the main phase with composition $Sr_{1.00}Fe_{0.87}Cu_{0.055}O_{2.84}$. The side phase with composition $Sr_{1.00}Fe_{0.64}Cu_{0.02}O_{2.43}$ could be a Cu-doped version of $Sr_3Fe_2O_7$ [50] or $Sr_3Fe_2O_5$ [51]. As those phases require hydrogen atmospheres for their reduction,[51] they are not expected to contribute significantly to the redox activity of the mixture in air.

A long term study did not show any degradation of the redox activity and mass change over 50 redox cycles (see supporting information Fig. S10), therefore, the reaction can be considered as completely reversible within the investigated temperature and oxygen partial pressure range. The particle size was virtually constant during all redox cycles, as annealing and breaking of the particles seemed in equilibrium (see SEM images in Supporting Information, Fig. S11-S13). The performance of the investigated samples is therefore expected to be persistent over a long term.The oxidation kinetics are shown in **Fig. 5**. Complete re-oxidation required less than one minute at temperatures of 350 °C and higher. At higher temperatures the reaction rates appear to be limited by the gas supply (gas flow rate: 100 mL/min).

High temperature X-Ray diffraction during reduction in air at 200 – 1000 °C showed a shift of reflections to lower 2ϑ values, which is attributed to an increase in interatomic distances upon reduction (see **Fig. 6**). The oxygen-deficient perovskite phase is stable over the whole temperature range. An additional reflection at 45° 2ϑ could not be assigned to known phases and might be attributed to the structural changes due to Cu doping or the Sr rich side phase mentioned before (see Supporting Information). This reflection appears in XRD scans of all Cu-doped samples in different intensity, and temperature-dependent intensity variations were found by *in-situ* XRD studies of $SrFe_{0.95}Cu_{0.055}O_{3-\delta}$.

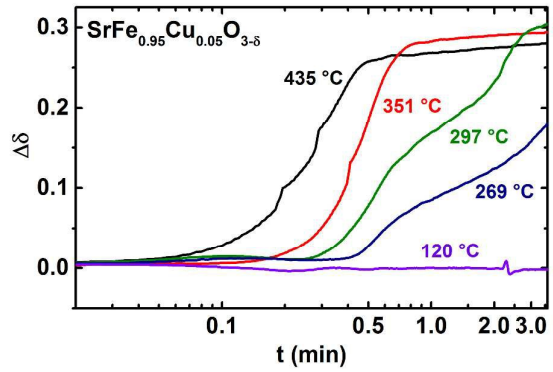

Fig. 5 Changes of the oxygen nonstoichiometry $\Delta\delta$ upon quick re-oxidation of $SrFe_{0.95}Cu_{0.05}O_{3-\delta}$ at different temperatures by switching the atmosphere from Ar 5.0 to a synthetic air/argon mixture with p_{O2} = 0.16.

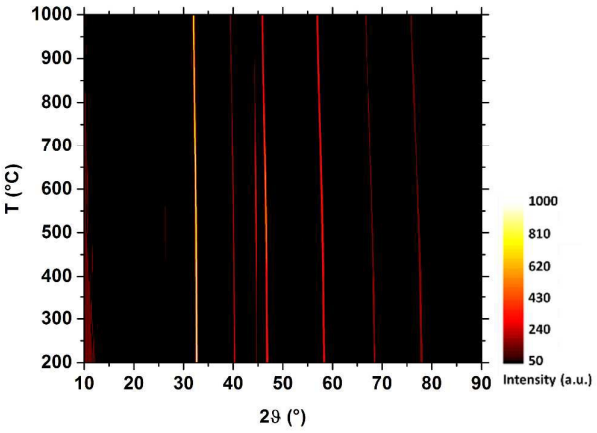

Fig. 6 In-situ XRD of $SrFe_{0.95}Cu_{0.055}O_{3-\delta}$ in ambient air at 200 – 1000 °C in steps of 40 °C showing the continuous shift of reflections to lower 2ϑ values, which is attributed to an increase in interatomic distances upon reduction without loss of the basic perovskite crystal structure.

Doping with Cr on the Fe site was also investigated, but lead to drastically decreased redox mass changes (0.57 % between 400/1000 °C, p_{O_2} = 0.16 bar, $SrCr_{0.1}Fe_{0.9}O_{3-\delta}$) and significantly increased interatomic distances in the oxidized state, which imply a higher nonstoichiometry of the oxidized form with respect to chromium-free strontium ferrite (see supporting information Fig. S17-S19).

(Sr,Ca)$MnO_{3-\delta}$

The synthesis of strontium manganites yielded dark black fine powders, whereas pure $CaMnO_{3-\delta}$ was formed as a fused substance with metallic appearance. According to XRD (see supporting information Fig. S7), single phase perovskites were formed. $CaMnO_3$ is most stable in a slightly distorted cubic structure, which was formed as expected (*Pnma,* space group 62). [52] $SrMnO_3$ is known in cubic and hexagonal modification, of which the hexagonal one is more stable at room temperature, owing to its tolerance factor of 1.04. [53, 54] The cubic phase is stable above 1400 °C and metastable in air at room temperature. It can be prepared at 1525 °C with subsequent quenching in air. [45] The hexagonal form of the $SrMnO_x$ perovskite was formed ($P6_3/mmc$, space group 194) using the calcination temperature program shown before.

The refined crystal parameters were consistent with literature values. [55] From XRD analysis and literature it can be concluded that the product was stoichiometric $SrMnO_3$ without oxygen deficiency. The expected reduction temperatures are high, [45] and thermogravimetric analysis up to a temperature of 1200 °C at p_{O_2} = 0.16 bar revealed mass changes of only 0.29 % (see supporting information Fig. S6).

$CaMnO_3$ is more difficult to reduce than $SrFeO_3$ (**Fig. 2**), and conversely has a stronger oxygen affinity. Partially reduced manganites will therefore have a stronger oxygen absorption than the corresponding ferrites, allowing lower oxygen partial pressures to be achieved.

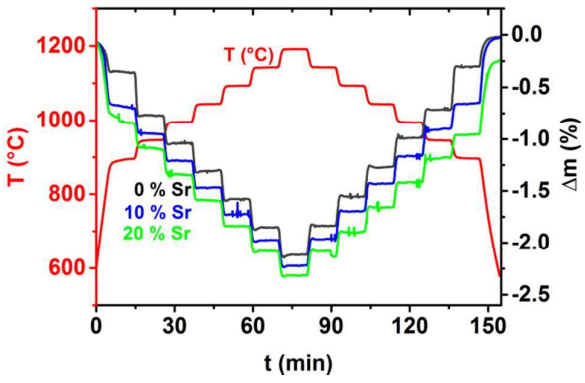

Fig. 7 Thermogravimetric analysis of $CaMnO_{3-\delta}$ (black), $Ca_{0.9}Sr_{0.1}MnO_{3-\delta}$ (blue), and $Ca_{0.8}Sr_{0.2}MnO_{3-\delta}$ (green) at p_{O2} = 0.16 bar. The exchange of Ca by 10 or 20 % Sr leads to an increased redox activity at T < 900 °C, and thus an increased overall redox activity in the range of 600 – 1200 °C.

Doping of $CaMnO_3$ was carried out with Sr on the Ca site and Cu or Fe on the Mn site. While Cu and Fe doping lead to decreased redox activities, Sr doping up to 20 % at the Ca site increased the redox mass change in a temperature window between 400 and 1200 °C at p_{O_2} = 0.16 bar. Doping with more than 20 % Sr lead to a decreased oxygen storage capacity with respect to pure $CaMnO_3$ (see **Fig. 10**). The redox mass changes of doped and undoped $CaMnO_{3-\delta}$ are displayed in **Fig. 7**. The reduction and oxidation were carried out in steps of 50 °C, showing the fast attainment of equilibrium after a temperature change. The addition of Sr leads to reduction onset at temperatures below 900 °C, which is attributed to an increased reducibility. According to powder XRD, the distorted cubic crystal structure of $CaMnO_3$ is maintained upon addition of Sr, and the distortion seems to decrease with increasing Sr content (see Supporting Information Fig. S8). According to literature, cubic $SrMnO_3$ can be reduced at lower temperatures than cubic $CaMnO_3$. [45] The addition of small amounts of Sr to the structure of $CaMnO_3$ is a feasible way to increase the oxygen storage capacity without losing reversibility. The reversibility was confirmed in long term studies with 50 redox cycles, where no degradation of $Ca_{0.8}Sr_{0.2}MnO_{3-\delta}$ was found (see supporting information Fig. S14). Particle sintering over the long term was observed only to a small extent (see SEM images in the Supporting Information, Fig. S15-S16).

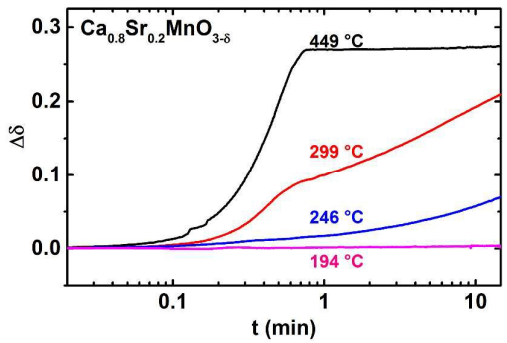

Fig. 8 Changes of the oxygen nonstoichiometry $\Delta\delta$ upon quick re-oxidation of $Ca_{0.8}Sr_{0.2}MnO_{3-\delta}$ at different temperatures by switching the atmosphere from Ar 5.0 to a synthetic air/argon mixture with p_{O2} = 0.16 bar.

Re-oxidation at p_{O2} = 0.16 bar occurs within seconds at temperatures of ~ 450 °C or higher (see **Fig. 8**). At 299 °C, the re-oxidation is half completed after 4 min. Even at 246 °C, a considerable re-oxidation reaction can be observed. While the reduction temperatures of ferrites and the manganites are different, the reaction speeds of the re-oxidations are comparable.

The lattice expansion upon reduction was studied via *in-situ* XRD (see **Fig. 9**), and refinement of the lattice parameters in space group 62 (*Pnma*). Above 600 °C the reduction begins (see thermogravimetric analysis), which corresponds to a stronger lattice expansion as oxide ions are removed from the lattice. This lattice expansion is referred to as 'chemical lattice expansion', whereas below 600 °C only the thermal expansion can be observed.

Journal Name

ARTICLE

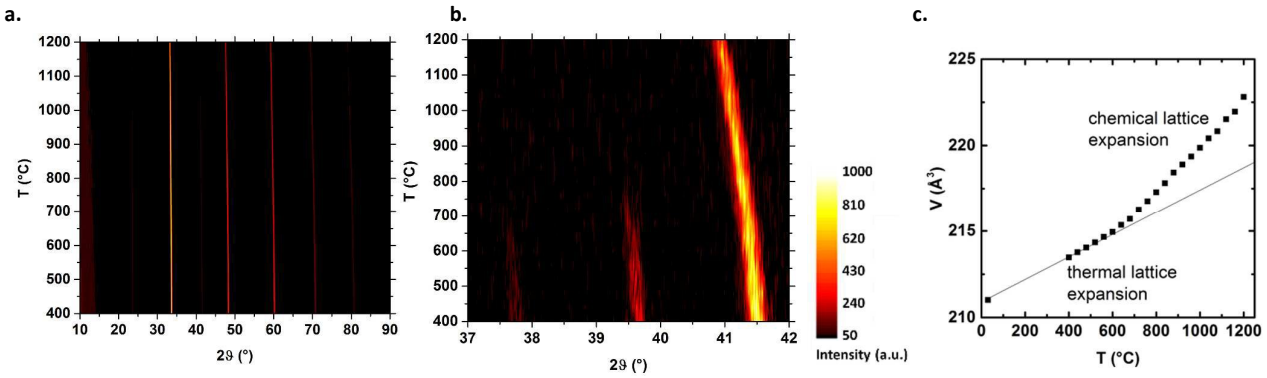

Fig. 9 *In-situ* XRD of $Ca_{0.8}Sr_{0.2}MnO_{3-\delta}$ in ambient air at 400 – 1200 °C in steps of 40 °C. a. the broad scan from 10 to 90 ° 2ϑ shows the temperature dependent shift of the reflections to lower 2ϑ angles, which is attributed to an expansion of the lattice. b. a detailed scan from 37 to 42 ° 2ϑ shows the disappearance of low intensity reflections, which is attributed to a decrease of the orthorhombic distortion. c. Data from a. refined in space group 62 showing a stronger lattice expansion during reduction at T > 600 °C.

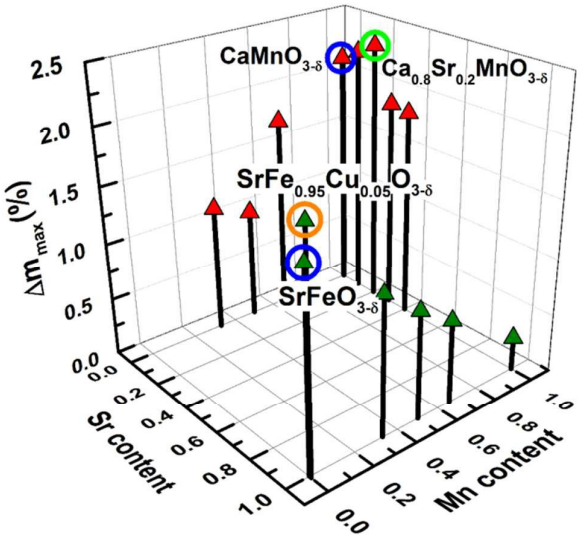

Fig. 10 Gravimetric oxygen storage capacity of (Ca,Sr) ferrites/manganites in relation to the Sr (= 1-Ca) and Mn content at an oxygen partial pressure of 0.16 bar. The Cu content is not shown. Red arrow heads: T = 400 - 1200 °C, green arrow heads: T = 400 - 1000 °C.

The chemical lattice expansion amounts to an increase of 2.1 % of the lattice volume between RT and 1200 °C in air, whereas the total lattice expansion increases the unit cell volume by 5.6 % in the same temperature window. Reflections with low intensity are attributed to the distortion of the ideal cubic structure. These reflections disappear at high temperatures upon reduction. This is attributed to the transition from orthorhombic to an undistorted cubic cell symmetry, probably with an intermediate tetragonal structure as described by other authors according to estimated tolerance factors. [56] The observed phase changes are completely reversible and lead only to a minor rearrangement of the metal cations upon reduction, thus allowing fast redox kinetics.

Mixed oxides and performance comparison

Mixed Mn-Fe oxides show oxygen storage capacities between the ones of pure ferrites and pure manganites. The oxygen storage capacities of the tested perovksites are compared in **Fig. 10**. The highest gravimetric oxygen storage capacity is achieved for $Ca_{0.8}Sr_{0.2}MnO_{3-\delta}$ and Cu-doped $SrFeO_{3-\delta}$. Moreover, while ferrites can be reduced almost to the brownmillerite state at T < 1000 °C and p_{O_2} = 0.16 bar, manganites require higher temperatures for their reduction, but also show a higher oxygen affinity in the reduced state, which should allow to reach lower oxygen partial pressures. By tuning the Mn or Fe content of the air separation materials, their oxygen affinity and reduction temperature can be tailored for each specific application. The choice of materials for air separation depends on the maximum tolerable oxygen content in the product stream, the maximum reachable temperature change rate, and the heat recovery efficiency.

Conclusions

We have demonstrated and studied the application of oxide perovskite materials for air separation and oxygen storage. A table showing the total list of perovskites that were synthesized and their

oxygen storage capacities can be found in the supporting information. The materials studied showed extraordinarily high reaction speeds due to the small phase changes upon reduction, which allows the transfer of larger amounts of oxygen per unit time with respect to binary oxide systems, e.g. based on Cu or Co. [57, 58] The reaction rates (complete reaction within seconds) and gravimetric oxygen storage capacities (over 2 % in air) are outstanding. [19, 20] If high heating and cooling rates can be achieved, the perovskite materials investigated herein can be used to separate large amounts of air per unit time and mass of oxides, solely using solar or waste heat as energy source. In addition, the two materials identified could be used in a cascade with $SrFe_{0.95}Cu_{0.05}O_{3-\delta}$ removing most of the oxygen from air followed by a further reduction in partial pressure using $Ca_{0.8}Sr_{0.2}MnO_{3-\delta}$.

Experimental Methods

All perovskite materials were prepared using a citric acid auto-combustion route involving metal ion complexation and citric acid decomposition, as described in the literature, [59,60] followed by a number of annealing steps with the final annealing at 1300 °C for 20 h. The sample preparation method is summarized in **Fig. 11**. Full details can be found in the Supporting Information.

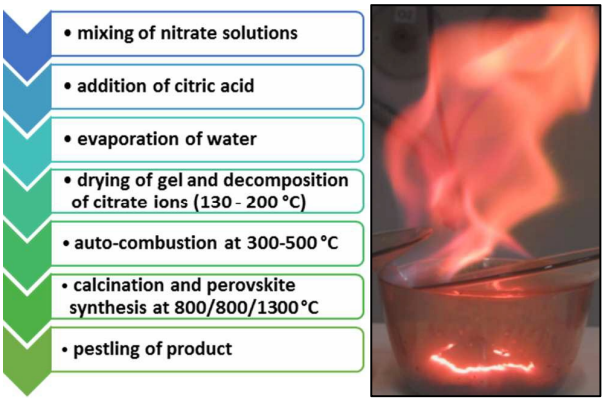

Fig. 11 Synthesis of perovskite materials via the citric acid auto-combustion route with a photo showing the reaction front traveling through the sample during the auto-combustion step.

X-Ray diffraction (XRD) experiments were carried out using a Siemens® D5000 diffractometer, which is equipped with a Cu-K_α X-Ray tube ($\lambda_{CuK\alpha} = 1.540598$ Å) and a secondary monochromator. Powdered samples were measured on Si single crystals in a range of 2ϑ = 10° to 90° scanned in steps of 0.01°. *In-situ* XRD experiments were carried out in atmospheric in steps of 40 °C using a high temperature chamber (Anton Paar GmbH, HTK 1200N) coupled to a Bruker D8 Discover diffractometer equipped with a Cu-K_α X-Ray tube and a Göbel mirror. Cell parameters were determined using the free software MAUD via Rietveld refinement using data of known phases in the literature as initial parameters. [61-63]

Phase analysis using energy dispersive X-Ray spectroscopy (EDS) was performed using pellets (5 mm diameter) pressed in a hydraulic press at 20 kN compression force, which were subsequently annealed in a muffle furnace for 10 h at 1300 °C. The pellets were cleaved and polished, then sputtered with Pt. EDS was performed using an Oxford INCA® X-Ray detector which is coupled to a Zeiss® Ultra-55 SEM system at an acceleration voltage of 15 kV.

For thermal analysis, a thermobalance system by Netzsch (Model STA 449 F3 Jupiter) equipped with a silicon carbide furnace was used, which can be operated in a temperature range from RT to 1550 °C with a maximum heating rate of 50 K/min. The powdered samples were placed on Pt sample holders mounted on ceramic pins. Ar 5.0 (Linde) was used as a protective gas, which was mixed with synthetic air (80:20 N_2:O_2 mol%, Linde) as a reaction gas (80:20 synthetic air : Ar), leading to an oxygen partial pressure of $p_{O_2} = 0.16$ bar. An empty scan was subtracted from each measurement as a reference.

To measure the reaction kinetics, the samples were reduced under Ar 5.0 at high temperatures, cooled down under Ar to lower temperatures, and then subjected to a mixture of synthetic air and Ar 5.0 with $p_{O_2} = 0.16$ bar.

Acknowledgements

This work has received funding from the Helmholtz Association in the framework of the Virtual Institute SolarSyngas (VH-VI-509) and from the DLR Programme Competition of Visions.

Notes and references

1. Shao, Z.; Haile, S. M., *Nature* **2004,** 431, (7005), 170-173.
2. Dong, F.; Chen, D.; Chen, Y.; Zhao, Q.; Shao, Z., *J. Mater. Chem.* **2012,** 22, (30), 15071-15079.
3. Nalbandian, L.; Evdou, A.; Zaspalis, V., *Int. J. Hydrogen Energy* **2011,** 36, (11), 6657-6670.
4. Scheffe, J. R.; Weibel, D.; Steinfeld, A., *Energy Fuels* **2013,** 27, (8), 4250-4257.
5. Jiang, Q.; Tong, J.; Zhou, G.; Jiang, Z.; Li, Z.; Li, C., *Sol. Energy* **2014,** 103, 425-437.
6. Lu, Y.; Zhao, H.; Chang, X.; Du, X.; Li, K.; Ma, Y.; Yi, S.; Du, Z.; Zheng, K.; Swierczek, K., *J. Mater. Chem. A* **2016,** 4, (27), 10454-10466.
7. Gür, T. M.; Belzner, A.; Huggins, R. A., *J. Membr. Sci.* **1992,** 75, (1), 151-162.
8. Bouwmeester, H. J. M.; Burggraaf, A. J., Chapter 10 Dense ceramic membranes for oxygen separation. In *Membr. Sci. Technol.*, Burggraaf, A. J.; Cot, L., Eds. Elsevier: 1996; Vol. Volume 4, pp 435-528.
9. Chang, C. C.; Weng, H. S., *Ind. Eng. Chem. Res.* **1993,** 32, (11), 2930-2933.
10. Jerndal, E.; Mattisson, T.; Lyngfelt, A., *Chem. Eng. Res. Des.* **2006,** 84, (9), 795-806.
11. Tanaka, H.; Misono, M., *Curr. Opin. Solid State Mater. Sci.* **2001,** 5, (5), 381-387.
12. Kim, C. H.; Qi, G.; Dahlberg, K.; Li, W., *Science* **2010,** 327, (5973), 1624-1627.
13. Johnsson, M.; Lemmens, P., Crystallography and Chemistry of Perovskites. In *Handbook of Magnetism and Advanced Magnetic Materials*, John Wiley & Sons, Ltd: 2007.

14. Colville, A. A.; Geller, S., *Acta Crystallographica Section B* **1971,** 27, (12), 2311-2315.
15. Shin, S.; Yonemura, M.; Ikawa, H., *Mater. Res. Bull.* **1978,** 13, (10), 1017-1021.
16. Hodges, J. P.; Short, S.; Jorgensen, J. D.; Xiong, X.; Dabrowski, B.; Mini, S. M.; Kimball, C. W., *J. Solid State Chem.* **2000,** 151, (2), 190-209.
17. Li, M.; Pietrowski, M. J.; De Souza, R. A.; Zhang, H.; Reaney, I. M.; Cook, S. N.; Kilner, J. A.; Sinclair, D. C., *Nat. Mater.* **2014,** 13, (1), 31-35.
18. Skinner, S. J.; Kilner, J. A., *Mater. Today* **2003,** 6, (3), 30-37.
19. Ezbiri, M.; Allen, K. M.; Gàlvez, M. E.; Michalsky, R.; Steinfeld, A., *ChemSusChem* **2015,** 8, (11), 1966-1971.
20. Motohashi, T.; Hirano, Y.; Masubuchi, Y.; Oshima, K.; Setoyama, T.; Kikkawa, S., Oxygen Storage Capability of Brownmillerite-type Ca2AlMnO5+δ and Its Application to Oxygen Enrichment. *Chem. Mater.* **2013,** 25, (3), 372-377.
21. Moghtaderi, B., Application of Chemical Looping Concept for Air Separation at High Temperatures. *Energy Fuels* **2010,** 24, (1), 190-198.
22. Felinks, J.; Lange, M.; Call, F., Thermochemical production of oxygen from air involves heating metal oxide by (in)direct concentrated solar radiation, and oxidizing metal oxide at lower temperature and in air atmosphere by partial/complete reduction of solar radiation. Patent DE102013209658A1: 2014.
23. Bülow, M.; Böer, J.; Burckhardt, W.; Guth, H. U.; Ullmann, H.; Vashook, V. V., Oxygen sorbent compositions and methods of using same. Patent US7347887B2: 2004.
24. N.N., Provisional Patent AU 2015905012: 2015.
25. Gayán, P.; Adánez-Rubio, I.; Abad, A.; de Diego, L. F.; García-Labiano, F.; Adánez, J., Development of Cu-based oxygen carriers for Chemical-Looping with Oxygen Uncoupling (CLOU) process. *Fuel* **2012,** 96, 226-238.
26. Dey, S.; Naidu, B. S.; Govindaraj, A.; Rao, C. N. R., *Phys. Chem. Chem. Phys.* **2015,** 17, (1), 122-125.
27. Galvez, M. E.; Jacot, R.; Scheffe, J.; Cooper, T.; Patzke, G.; Steinfeld, A., *Phys. Chem. Chem. Phys.* **2015,** 17, (9), 6629-6634.
28. Stokes, R., *Building Upon Air: A History of the International Industrial Gases Industry from the 19th to the 21st Centuries*. Cambridge University Press: 2015.
29. Call, F.; Felinks, J.; Lange, M. Solare Ammoniakproduktion. Patent DE102014213987A1: 2014.
30. Hänchen, M.; Stiel, A.; Jovanovic, Z. R.; Steinfeld, A., *Industrial & Engineering Chemistry Research* **2012,** 51, (20), 7013-7021.
31. Erisman, J. W.; Sutton, M. A.; Galloway, J.; Klimont, Z.; Winiwarter, W., *Nat. Geosci.* **2008,** 1, (10), 636-639.
32. Chen, Z.; Ran, R.; Shao, Z.; Yu, H.; Costa, J. C. D. d.; Liu, S., *Ceram. Int.* **2009,** 35, (6), 2455-2461.
33. Klimkowicz, A.; Świerczek, K.; Takasaki, A.; Dabrowski, B., *Solid State Ionics* **2014,** 257, 23-28.
34. Jain, A.; Ong, S. P.; Hautier, G.; Chen, W.; Richards, W. D.; Dacek, S.; Cholia, S.; Gunter, D.; Skinner, D.; Ceder, G.; Persson, K. A., *APL Mater.* **2013,** 1, (1), 011002.
35. Jain, A.; Hautier, G.; Ong, S. P.; Moore, C. J.; Fischer, C. C.; Persson, K. A.; Ceder, G., *Phys. Rev. B* **2011,** 84, (4), 045115.
36. Jain, A.; Hautier, G.; Moore, C. J.; Ping Ong, S.; Fischer, C. C.; Mueller, T.; Persson, K. A.; Ceder, G., *Comp. Mater. Sci.* **2011,** 50, (8), 2295-2310.
37. Wiberg, E.; Wiberg, N., *Inorganic Chemistry*. Academic Press: 2001.
38. Levason, W.; Spicer, M. D., *Coord. Chem. Rev.* **1987,** 76, 45-120.
39. Darracq, S.; Kang, S. G.; Choy, J. H.; Demazeau, G., *J. Solid State Chem.* **1995,** 114, (1), 88-94.
40. Wu, X. J.; Laffez, P.; Yamauchi, H.; Môri, N., *Phys. C (Amsterdam, Neth.)* **1994,** 228, (3), 292-298.
41. JANAF THERMOCHEMICAL TABLES Third Edition. *Anal. Chem.* **1990,** 62, (10), 588A-588A.
42. Chase, M. W.; National Institute of, S.; Technology, *NIST-JANAF thermochemical tables*. American Chemical Society ; American Institute of Physics for the National Institute of Standards and Technology: [Washington, D.C.]; Woodbury, N.Y., 1998.
43. Schmidt, M.; Campbell, S. J., *J. Phys. Chem. Solids* **2002,** 63, (11), 2085-2092.
44. Takeda, Y.; Kanno, K.; Takada, T.; Yamamoto, O.; Takano, M.; *J. Solid State Chem.* **1986,** 63, (2), 237-249.
45. Rørmark, L.; Mørch, A. B.; Wiik, K.; Stølen, S.; Grande, T., *Chem. Mater.* **2001,** 13, (11), 4005-4013.
46. Takeda, Y.; Naka, S.; Takano, M.; Shinjo, T.; Takada, T.; Shimada, M., *Mater. Res. Bull.* **1978,** 13, (1), 61-66.
47. Gibb, T. C.; Herod, A. J.; Munro, D. C.; Peng, N., Synthesis under high pressure and characterisation by Mossbauer spectroscopy of non-stoichiometric Ca2Fe2O5.12. *Journal of Materials Chemistry* **1994,** 4, (9), 1451-1455.
48. Deganello, F.; Liotta, L. F.; Longo, A.; Casaletto, M. P.; Scopelliti, M., *J. Solid State Chem.* **2006,** 179, (11), 3406-3419.
49. Shannon, R., *Acta Crystallogr. Sect. A: Found. Adv.* **1976,** 32, (5), 751-767.
50. Maljuk, A.; Strempfer, J.; Ulrich, C.; Sofin, M.; Capogna, L.; Lin, C. T.; Keimer, B., Growth of Sr3Fe2O7−x single crystals by the floating zone method. *J. Cryst. Growth* **2004,** 273, (1–2), 207-212.
51. Yamamoto, T.; Tassel, C.; Kobayashi, Y.; Kawakami, T.; Okada, T.; Yagi, T.; Yoshida, H.; Kamatani, T.; Watanabe, Y.; Kikegawa, T.; Takano, M.; Yoshimura, K.; Kageyama, H., Pressure-Induced Structural, *J. Am. Chem. Soc.* **2011,** 133, (15), 6036-6043.
52. Melo Jorge, M. E.; Correia dos Santos, A.; Nunes, M. R., *Int. J. Inorg. Mater.* **2001,** 3, (7), 915-921.
53. Yusa, H.; Sata, N.; Ohishi, Y., *Am. Mineral.* **2007,** 92, (4), 648-654.
54. Khomskii, D. I., *Transition Metal Compounds*. Cambridge University Press: 2014.
55. Battle, P. D.; Gibb, T. C.; Jones, C. W., *J. Solid State Chem.* **1988,** 74, (1), 60-66.
56. Dabrowski, B.; Chmaissem, O.; Mais, J.; Kolesnik, S.; Jorgensen, J. D.; Short, S., *J. Solid State Chem.* **2003,** 170, (1), 154-164.
57. Block, T.; Schmücker, M., *Sol. Energy* **2016,** 126, 195-207.
58. Motuzas, J.; Diniz da Costa, J. C., *Journal of Materials Chemistry A* **2015,** 3, (33), 17344-17350.
59. Danks, A. E.; Hall, S. R.; Schnepp, Z., *Mater. Horiz.* **2016**.
60. Barbooti, M. M.; Al-Sammerrai, D. A., *Thermochim. Acta* **1986,** 98, 119-126.
61. Lutterotti, L.; Vasin, R.; Wenk, H.-R., *Powder Diffr.* **2014,** 29, (01), 76-84.
62. Lutterotti, L.; Chateigner, D.; Ferrari, S.; Ricote, J., *Thin Solid Films* **2004,** 450, (1), 34-41.
63. MAUD, *Materials Analysis Using Diffraction, Version 2.55,* **2015**.

Table of Contents entry

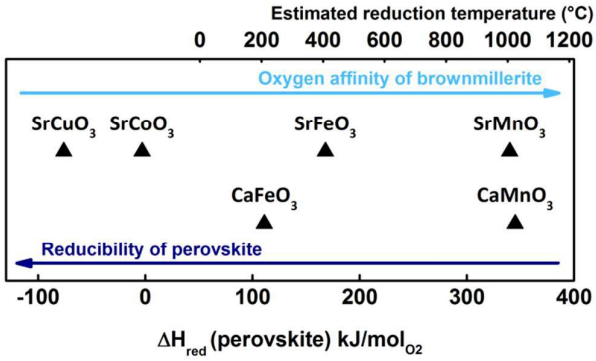

A materials screening of perovskites for oxygen storage applications yielding two promising materials, $SrFe_{0.95}Cu_{0.05}O_{3-\delta}$ and $Ca_{0.8}Sr_{0.2}MnO_{3-\delta}$ with outstanding performance.